

GEOFISICA INTERNACIONAL

REVISTA DE LA UNION GEOFISICA MEXICANA, AUSPICIADA POR EL INSTITUTO DE
GEOFISICA DE LA UNIVERSIDAD NACIONAL AUTONOMA DE MEXICO

Vol. 25

México, D. F., 1o. de julio de 1986

Núm. 3

NEW FORMULAE FOR LINEAR TRAVEL TIME INVERSION IN 2-D HETEROGENEOUS MEDIA. THEORY AND RESULTS

J. A. MADRID*

(Received: June 17, 1985)

(Accepted: December 5, 1985)

RESUMEN

Se desarrollan fórmulas para el cálculo de residuos de tiempo de recorrido y derivadas parciales con respecto a la velocidad de propagación de onda definida en un punto, para modelos de la Tierra en dos dimensiones. Las derivadas están completamente determinadas por las trayectorias (rayos). Los residuos del tiempo de recorrido son tan exactos como los tiempos observados y no es necesario resolver el problema típico de extremos fijos. Se introduce un nuevo tipo de inversión que actúa directamente sobre las líneas de igual velocidad, haciendo posible la inspección visual inmediata de los resultados obtenidos durante una iteración.

Se usaron datos sintéticos correspondientes a varios modelos para probar la validez de las fórmulas desarrolladas, con excelentes resultados. La forma de tratar un problema particular depende tanto de los datos disponibles como de la estructura buscada.

* *División de Ciencias de la Tierra, Centro de Investigación Científica y Educación Superior de Ensenada, B. C. MEXICO.*

ABSTRACT

Reliable formulae for the computation of travel time residuals and partial derivatives for the inverse problem in two dimensions based on ray tracing are developed. The partial derivatives are completely determined by the path and the travel time residuals are as accurate as the observed travel times; it is not necessary to solve the traditional 'fixed ends problem'. A new kind of inversion is introduced that operates directly on the shape of the isovelocity lines, making possible the immediate visual inspection of the results of an iteration.

The formulae were checked against synthetic data corresponding to a variety of models. The way to approach a particular problem depends both on the available data and the structure.

INTRODUCTION

Lateral variations of earth structure have become of great interest both for geologists and geophysicists, especially when studies of the crust are undertaken. Methods for inverting seismic data have been reported that include hypocenter relocation and reparameterization of the medium, either continuous or discrete (*c.f.* Spencer and Gubbins (1980), Firbas (1981), Thurber (1980)). All these methods are based on ray tracing by various approaches, for example Cerveny, Molotkov and Pšencik, 1977, or Pereyra *et al.*, 1980. Particularly interesting is Firbas (1981), because he uses continuous analytical functions to describe the velocity of propagation, although this method is limited to laterally homogeneous starting models. In other method (Thurber, 1980) the partial derivatives depend on the number of points used to interpolate the velocity, and these points change even for close-by rays. All methods require the determination of the travel time at a certain number of points of observation, i.e., the solving of the so-called 'two-points ray tracing' or 'fixed ends extremal travel time' problem. In this paper we relax such requirement and use a second order correction to the travel time of a ray emerging close to an observation point. Finally, we introduce a new approach to the inversion procedure that we call 'non-rigid inversion'. This kind of inversion acts directly upon the position of isovelocity lines, thus making the visualization of the result of each iteration fast and easy. We believe that in this way some control on the successive steps of inversion is achieved, making it more active and dynamic.

THEORY

In this section, we will obtain an expression for the partial derivative of the travel time corresponding to a ray path with respect to a point velocity, starting with the ray-tracing technique known as 'circular approximation' (Gebrande (1976), Aric and Sailer (1980) or Madrid and Traslosheros (1983)).

Consider a triangular region S bounded by the lines joining vertices v_1 , v_2 and v_3 (Fig. 1). We assume that inside this region the velocity of propagation of a wave is

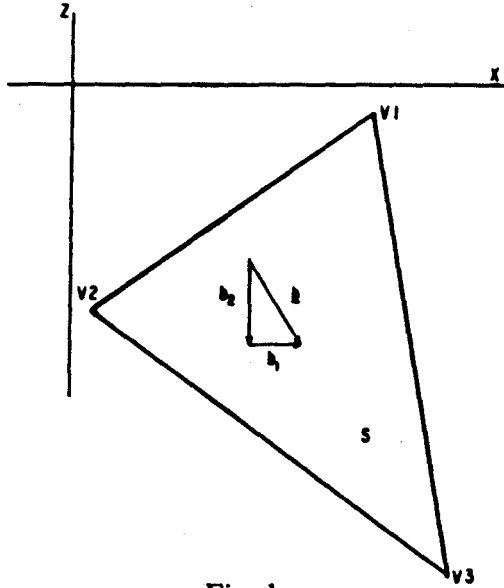


Fig. 1

linear in the 'absolute' or 'external' coordinates, x , z . Thus we can write

$$v(x, z) = v_0 + b_1 x + b_2 z \tag{1}$$

$(x, z) \in S$. The corresponding equations for the velocities at the vertices are

$$\begin{aligned} v_1 &= v_0 + b_1 x_1 + b_2 z_1 \\ v_2 &= v_0 + b_1 x_2 + b_2 z_2 \\ v_3 &= v_0 + b_1 x_3 + b_2 z_3 \end{aligned} \tag{2}$$

Equations (2) may be solved by Kramer's rule to yield the values of v_0 , b_1 , b_2 :

$$\begin{aligned} b_1 &= \frac{D(1, v, z)}{A} \\ b_2 &= \frac{D(1, x, v)}{A} \\ v_0 &= \frac{D(v, x, z)}{A} \end{aligned} \tag{3}$$

where $A = D(l, x, z)$ is the determinant of the system and $D(l, v, z)$, $D(l, x, v)$ and $D(v, x, z)$ are the auxiliary determinants. It is easy to see that A is twice the area of the region S .

Let us analyze the case $b_1 = 0$, $b_2 = -b$; i.e., the velocity is laterally homogeneous, but increases with depth:

$$v = v_0 + b_2 z \quad (4)$$

As is well known, in such a medium, every ray is characterized by a ray parameter 'p' that is constant along the path. The ray parameter is the horizontal component of the slowness vector:

$$\underline{u} = (p, q) = \frac{1}{v} \cos\theta, \sin\theta \quad (5)$$

and the path is a circular arc of radius of curvature

$$R = \frac{-1}{pb} \quad (6)$$

In a medium with both $b_1 = 0$, $b_2 = 0$ (Fig. 2) the vector gradient is tilted with respect to the vertical axis by an angle

$$r = -\tan^{-1} \left(\frac{b_1}{b_2} \right) \quad (7)$$

so that performing a rotation of the original axis (x, z) by an angle r , as indicated in the figure, we obtain a velocity gradient and slowness components

$$\begin{aligned} \underline{b}' &= (0, b_2') \\ p' &= p \cos r + q \sin r \\ q' &= -p \sin r + q \cos r \end{aligned} \quad (8)$$

where $b' = -b = (b_1^2 + b_2^2)^{1/2}$.

The (x', z') system is called the 'local system'. From the figure, it is clear that

$$\begin{aligned} \cos r &= \frac{b_1}{b} \\ \sin r &= \frac{b_2}{b} \end{aligned} \quad (9)$$

since in the local system $v = v(z')$ and $p' = \text{const}$, in analogy with (6):

$$R = \frac{1}{p'b'}$$

(10)

$$= (-pb_2 + qb_1)^{-1} = \text{const}$$

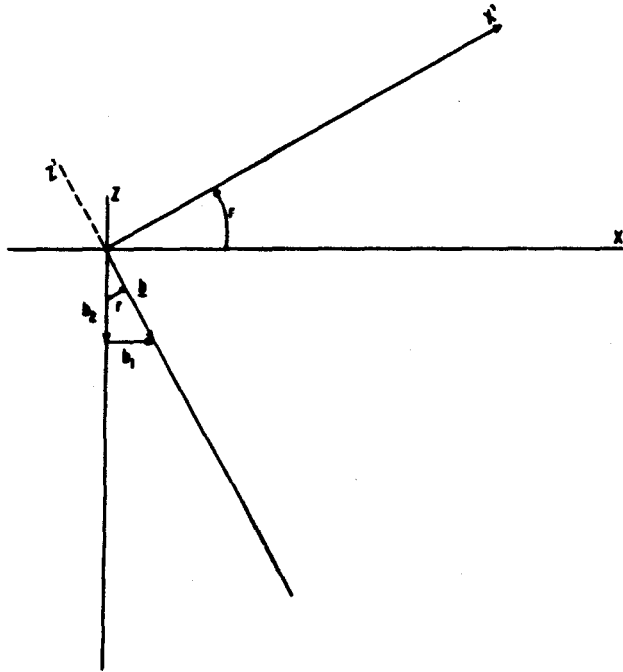


Fig. 2. Rotation by angle r that transforms velocity $v = v_0 + b_1x + b_2z$ in $v = v_0' + b'z'$.

Suppose that a ray travels from P_0 to P_f in a triangular region S , as shown in Fig.

3. The travel time is

$$\Delta T = \int \frac{dS}{v} \tag{11}$$

where $dS = R d\theta$ and R is given by (10). The problem we are concerned with may be stated as follows:

What is the change in travel time ΔT for a ray if we perturb, say, the velocity v , by a small fraction, v_3 ?; i.e., we perturb the model and want to see how much the perturbation alters the travel time of a ray.

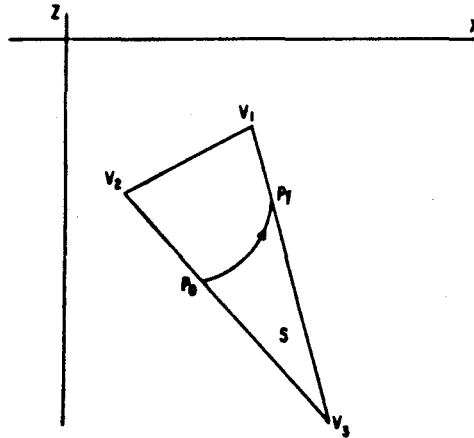


Fig. 3. Example of a circular path in S from Po to Pf.

The change in ΔT may be expressed as:

$$\delta(\Delta T) = -\delta v_3 \int \frac{\partial v}{\partial v_3} \frac{dS}{v^2} \quad (12)$$

to integrate this expression, the partial derivative $\partial v / \partial v_3$, must be determined. To achieve this let us perturb equations (2) according to the assumption

$$\begin{aligned} \delta v_1 &= 0 = \delta v_0 + x_1 \delta b_1 + z_1 \delta b_2 \\ \delta v_2 &= 0 = \delta v_0 + x_2 \delta b_1 + z_2 \delta b_2 \\ \delta v_3 &= \delta v_0 + x_3 \delta b_1 + z_3 \delta b_2 \end{aligned} \quad (13)$$

Again, these equations are easily solved with the aid of Kramer's rule, yielding

$$\begin{aligned} \delta b_1 &= \left(\frac{D}{A} \right) \sin \alpha \delta v_3 \\ \delta b_2 &= - \left(\frac{D}{A} \right) \cos \alpha \delta v_3 \\ \delta v_0 &= \left(\frac{D}{A} \right) Z_D^\alpha \delta v_3 \end{aligned} \quad (14)$$

where D is the length of the side of the triangle opposite to the perturbed vertex, α is the angle of this side with the x -axis. A is the same determinant as in (2), and Z_D^α is the z -coordinate in a system rotated by an angle α , so that D becomes parallel with

the X^α axis (Figure 4); Z_D^α is the Z coordinate for the line D . Dividing by δv_3 and taking the limit as $\delta v_3 \rightarrow 0$, we get

$$\frac{\partial b_1}{\partial v_3} = \left(\frac{D}{A}\right) \sin \alpha \delta v_3$$

$$\frac{\partial b_2}{\partial v_3} = -\left(\frac{D}{A}\right) \cos \alpha \delta v_3 \tag{15}$$

$$\frac{\partial v_0}{\partial v_3} = \left(\frac{D}{A}\right) Z^\alpha \delta v_3$$

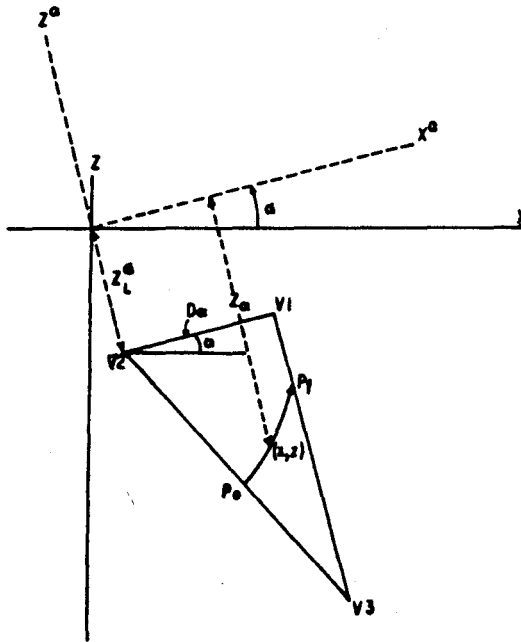


Fig. 4. The (X^α, Z^α) coordinate system is obtained by rotating the external system to align D with X^α .

To obtain the partial derivative $\partial v/\partial v_3$, a small increment in velocity is taken along the ray path:

$$\delta v = \delta v_0 + x \delta b_1 + z \delta b_2 \tag{16}$$

dividing by δv_3 and taking the limit as $\delta v_3 \rightarrow 0$:

$$\frac{\partial v}{\partial v_3} = \frac{\partial v_0}{\partial v_3} + x \frac{\partial b_1}{\partial v_3} + z \frac{\partial b_2}{\partial v_3} \tag{17}$$

that, by (15) reduces to

$$\frac{\partial v}{\partial v_3} = \frac{D}{A} (Z_D^\alpha - Z) \quad (18)$$

where Z is the Z^α coordinate along the ray path, in the (X^α, Z^α) system. Note that, at $Z = Z_D^\alpha$, $\delta v = 0$, whereas at $Z = Z_D^\alpha - h$, $\delta v = \delta v_3$, with h = the height of the triangle if D is taken as its basis. Both results agree with (13). Expression (12) then becomes:

$$\frac{\partial \Delta T}{\partial v_3} = -\frac{D}{A} \int (Z_D^\alpha - Z) \frac{dS}{v^2} \quad (19)$$

To evaluate this expression, we use the fact that $dS/v^2 = dq'/b$, so that integral (19) may be written as

$$\frac{\partial \Delta T}{\partial v_3} = \frac{-D}{bA} \int (Z_D^\alpha - Z) dq' \quad (20)$$

which may be integrated by parts:

$$\int (Z_D^\alpha - Z) dq' = \Delta [(Z_D^\alpha - Z)q'] + \int q' dZ$$

now, using $dZ = -dx' \sin(r - \alpha) + dz' \cos(r - \alpha)$, the integral in the right side is

$$\begin{aligned} \int q' (-dx' \sin(r - \alpha) + dz' \cos(r - \alpha)) \\ = \cos(r - \alpha) [\Delta \tau] - p' \sin(r - \alpha) \int dz' \end{aligned}$$

where $\tau = T - pX$ is the 'Tau' function or time intercept, so that finally we have, for (19):

$$\begin{aligned} \frac{\partial \Delta T}{\partial v_3} = & - (D/bA) \cos(\alpha - r) [\Delta T] + (Dp'/bA) [\Delta X] \\ & - (D/bA) \Delta [q'(Z_D^\alpha - Z)] \end{aligned} \quad (21)$$

Expression (21) gives the rate of change of travel time of any ray that passes through the triangular region. Note that perturbing one of the vertices implies perturbing as many as six neighbouring regions as well (Fig. 5), so that the effect of them all must be included if necessary. The travel time for the ray in figure 5 is

$$T = \sum_i \Delta T_i \quad (22)$$

where $i = 1, 2, \dots, n$ is the index of the circular segments along the path. We wish to determine

$$\frac{\partial T}{\partial v_k}$$

i.e., the rate of change in travel time as v_k changes. By (22), one gets

$$\frac{\partial T}{\partial v_k} = \sum_{li=A,B,C,D} \frac{\partial \Delta T_{li}}{\partial v_k} \quad (23)$$

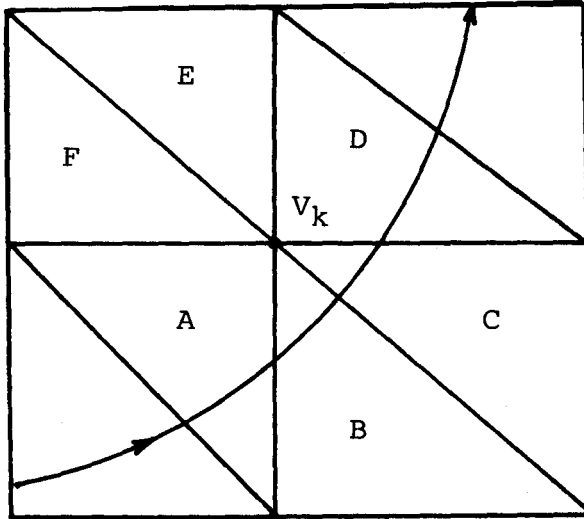


Fig. 5. Regions A, B, C, D, E, and F that are affected by a perturbation of point velocity v_k .

all other terms are null. Expressions (21) and (23), and knowledge of the ray path is all that is necessary to compute the partial derivatives required for the procedure of inversion.

To complete the inversion scheme, the travel time residual δT must be calculated. To be rigorous, the problem of fixed ends ray tracing should be solved. However, a second order correction to the travel time for a ray that emerges reasonably close to the point of observation will prove to be sufficient. Of course, this depends on the deviations of the model being 'small', that is, travel time variations are of the second order compared with variations of the raypath.

Figure 6 shows a ray in the guessed model which emerges at X_p , very close to an observation distance X_{obs} . At merging point, the ray is characterized by T_p , p , q , the travel time and the slowness components evaluated at the surface $x = X_p$, $z = 0$.

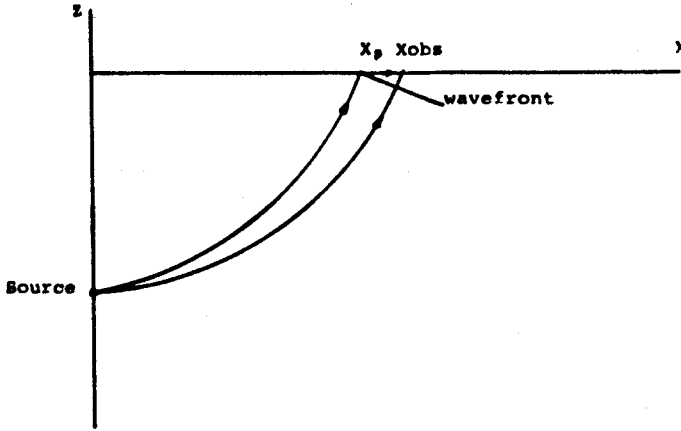


Fig. 6. Example of a ray in an assumed model arriving at X_p .

To reach the observation distance, the wavefront must spend an extra time

$$T_c = \int p(X) dX \quad (24)$$

as its intercept with the surface travels from X_p to X_{obs} . At $x = X_{obs}$, $z = 0$, both the intercept and the point on the ray traveling inside the medium coincide, and so do their total travel times. If the variation of $p(X)$ is known, the time correction (24) is exact. Since generally this is not the case, we evaluate this integral approximately expanding $p(X)$ up to the linear term:

$$\begin{aligned} p(X, z=0) &= p(X_p) + \left(\frac{dp}{dX}\right)(X - X_p) + \dots \\ &= p(X_p) + \left(\frac{dp}{dX}\right)(X - X_p) \end{aligned}$$

The factor (dp/dX) may be obtained as follows: in the local system, the horizontal slowness p' is conserved. In going from Po' to Pf' , q' changes due to the change in local depth z' ; to first order:

$$q'(zf') = qo' + \left(\frac{dq'}{dz'}\right) dz'$$

by
$$\frac{1}{v^2} = p'^2 + q'^2, \quad p' = \text{const}$$

we get
$$\frac{dq'}{dz'} = \frac{1}{q'v^3} \frac{dv}{dz'} = \frac{b}{q'v^3}$$

so that
$$qf' = qo' + \left(\frac{b}{q'v^3}\right) dz' \quad (25)$$

the slowness vector at the final point is (pf', qf') . The rotation may be inverted to get:

$$\begin{aligned} pf &= p_0 + \frac{\partial p}{\partial x} dx + \frac{\partial p}{\partial z} dz \\ &= p' \cos r - qf' \sin r \\ &= p_0 - \left(\frac{1}{qf' v^3} \right) (-dx \sin r + dz \cos r) \sin r \\ &= p_0 + \left(\frac{b_1}{qf' v^3 b} \right) dx - \left(\frac{b_1 b_2}{qf' v^3} \right) dz \end{aligned}$$

From these expressions, it is seen that:

$$\begin{aligned} \frac{\partial p}{\partial x} &= \frac{b_1^2}{q' v^3 b} \\ \frac{\partial p}{\partial z} &= \frac{-b_1 b_2}{q' v^3 b} \end{aligned} \tag{26}$$

with similar relations for $\partial q/\partial x$ and $\partial q/\partial z$. Then the travel time correction is:

$$\begin{aligned} T_c &= \int (p + \left(\frac{dp}{dX} \right) (X - X_p)) dX \\ &= p(X_{obs} - X_p) + \left(\frac{b_1}{2q' v^3} \right) (X_{obs} - X_p)^2 \end{aligned} \tag{27}$$

The residual at X_{obs} is then

$$\delta T = T_{obs} - T_p - T_c \tag{28}$$

The correction term includes the term used by Wiggins and Madrid (1974), Wiggins (1976), and later by Chapman (1978) and Chapman and Drummond (1982) in the computation of synthetic seismograms. In the present study this term prevents the solving of the fixed ends problem.

Once the residuals and the partial derivatives have been determined, the procedure of inversion is standard (*c.f.* Wiggins (1972), Jackson (1972)). In the following section, computational experiments and their results are explained.

COMPUTATIONAL EXPERIMENTS AND DISCUSSION OF RESULTS

In this section, we report the results obtained from applying the theory developed in the last section to a variety of models. The examples were run as follows: first, a laterally heterogeneous 'actual' model was established, and a number of travel times and observation points (ranges) were selected by exact ray tracing. Then a laterally homogeneous model was designed to perform the inversion. This initial (assumed) model was sampled by the shooting method to determine adequate limits for the shooting angles. The computer program was fixed to automatically select the rays emerging closest to the previously selected observation ranges, and the partial derivatives and time correction were computed for each selected ray.

Two different shooting procedures were used. The first consisted of shooting the same number of rays (fifty or a hundred in different trials) and repeating the automatic selection scheme in each iteration; the second was to keep the initial take off angle of each selected ray for further iterations. The first procedure was found more accurate, albeit more time consuming. Nevertheless, this is not a serious drawback, since the circular approximation is extremely fast and cheap. Although all the examples start with a laterally homogeneous model, this is not a restriction, and we could as well have started with a laterally heterogeneous model.

Six different models were tried with a fixed source. The original models 1 and 2 (Figure 7) are actually the same, but model 2 was generated by discretizing model 1 with nine points. Model 1 was inverted twice: first, using two and then four rays (determined and overdetermined problem), finding no difference at all. The velocity at the two upper points was kept fixed. In model 2 the six lower points were allowed to vary. Figure 8 shows the convergence history of rays, residuals and isovelocity lines for both models. The convergence was perfect (null residuals). The main difference found was the number of iterations required for convergence, four for the first model, eleven for the second. The values taken by the variables in successive iterations are shown in Table I.

Model 3 is shown in Figure 9(a) together with its isovelocities and rays arriving at selected observation points. In this model all four points could vary. As in the previous example, convergence was perfect. It was observed that inclusion of the second order term in (27) accelerated the convergence. In this example, five iterations were required when this term was left out, whereas when it was included only three

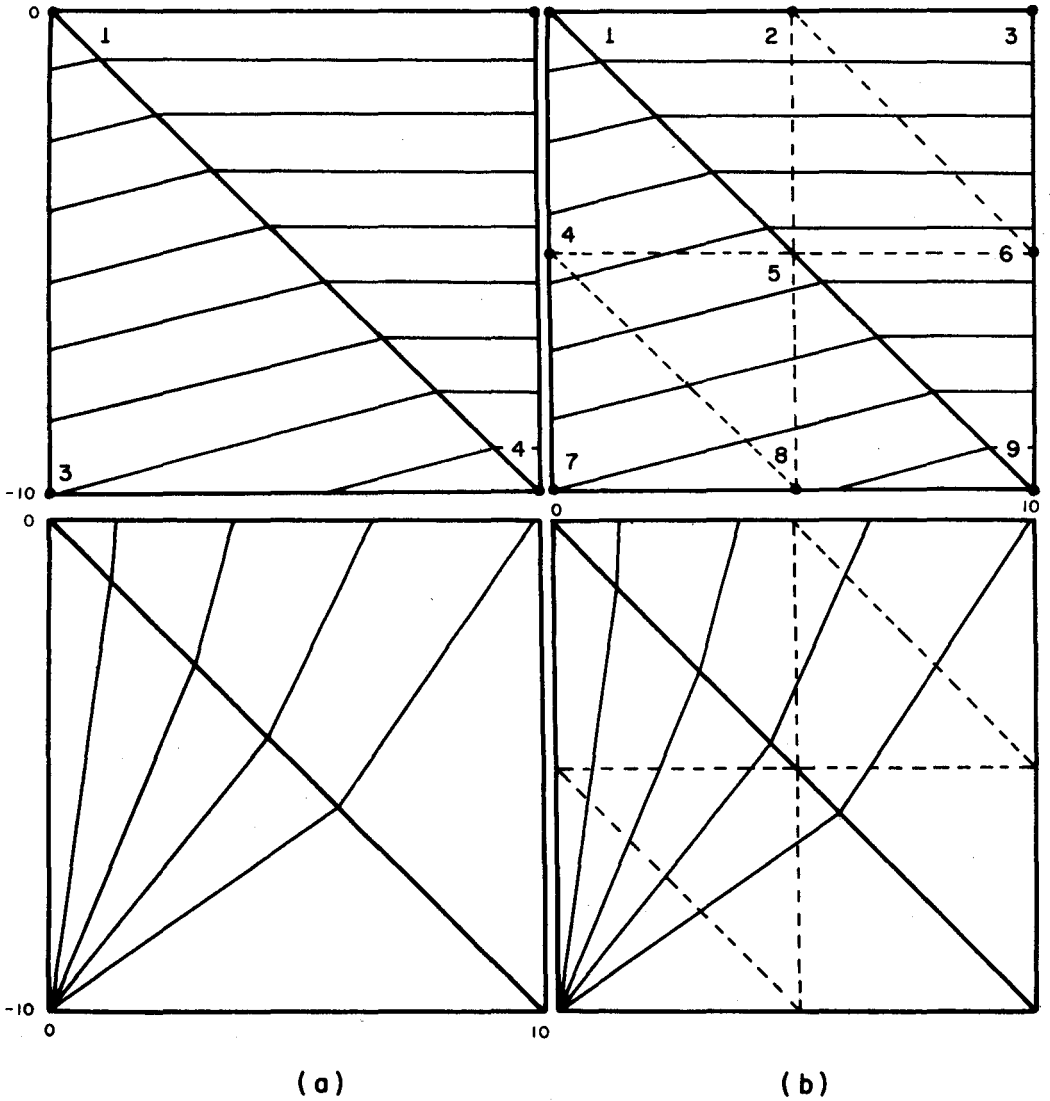


Fig. 7. (a) Model 1 is specified by the four corner points of the square. Only points 3 and 4 were allowed to vary. (b) Model 2 is specified by 9 points with interpolated values for points 2, 4, 5, 6 and 8. Points 4 to 9 were allowed to vary. The velocity of the starting model was 3.0 at the top ($z=0$), 7.0 at the bottom ($z=-10$). The size of the model are 10 x 10 square units.

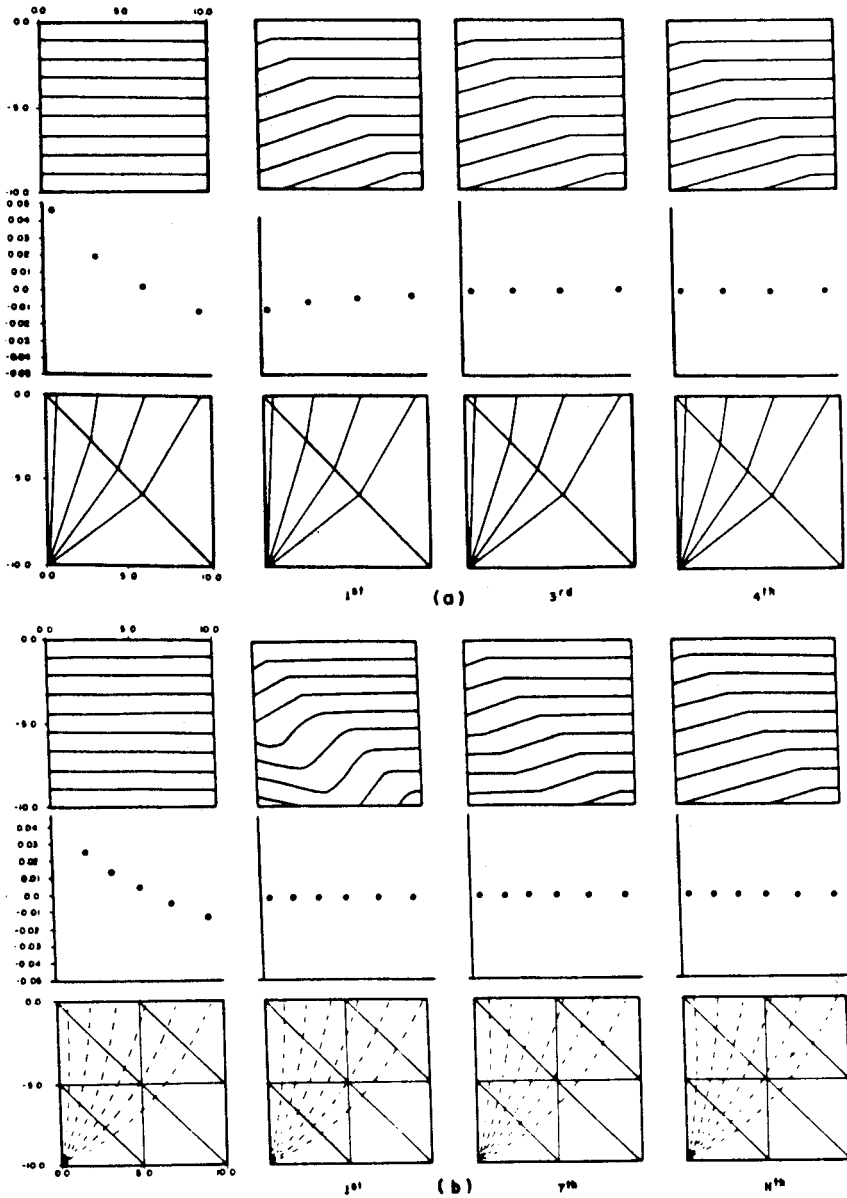


Fig. 8. (a) Convergence of model 1. (b) Convergence of model 2. The figures shown correspond to iterations 3, 7, and 11. In (a) the rays were not interpolated.

T A B L E I

IT	MOD 1		MOD 2					
	V3	V4	V4	V5	V6	V7	V8	V9
1	6.380	7.443	4.352	5.325	5.340	6.817	6.627	7.302
2	6.495	7.403	4.650	5.095	5.082	6.860	7.093	7.433
3	6.500	7.400	4.651	5.180	5.180	6.840	6.835	7.375
4	6.500	7.400	4.645	5.181	5.180	6.839	6.848	7.367
5			4.647	5.179	5.178	6.840	6.852	7.371
6			--	--	--	--	--	--
7			--	--	--	--	--	--
8			4.693	5.197	5.197	6.672	6.811	7.380
9			4.741	5.201	5.201	6.524	6.935	7.396
10			4.750	5.200	5.200	6.500	6.950	7.400
11			4.750	5.200	5.200	6.500	6.950	7.400

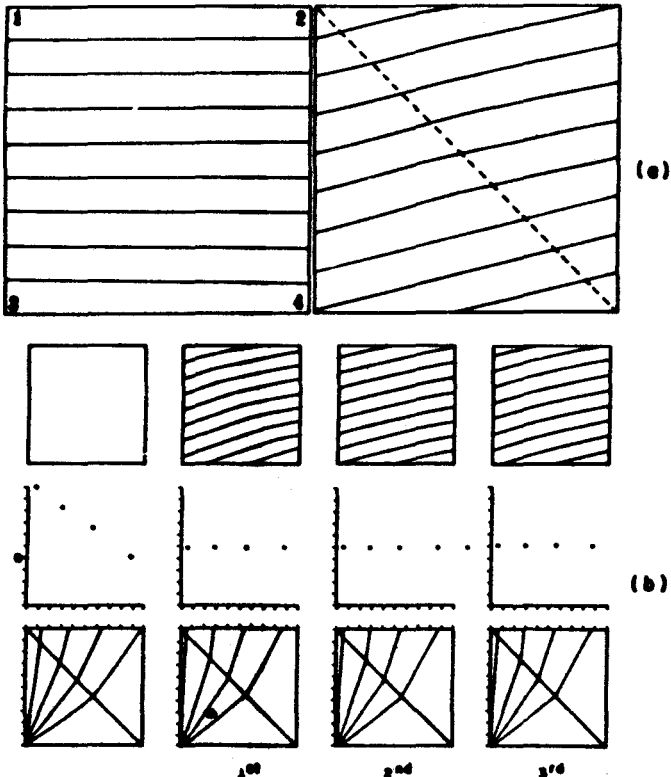
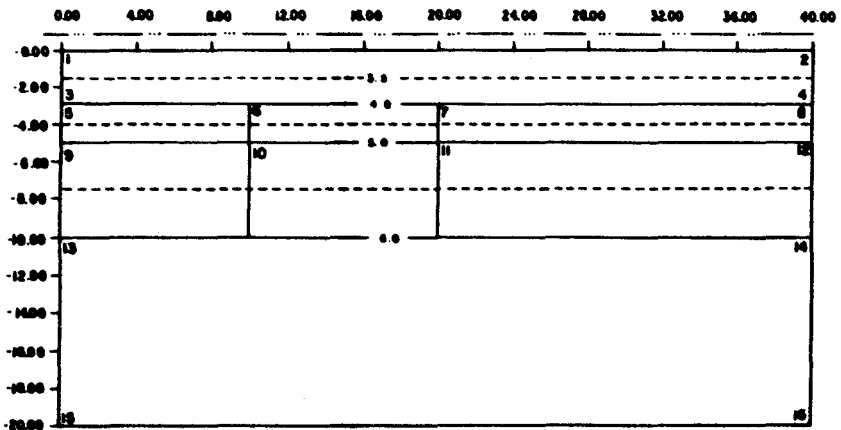


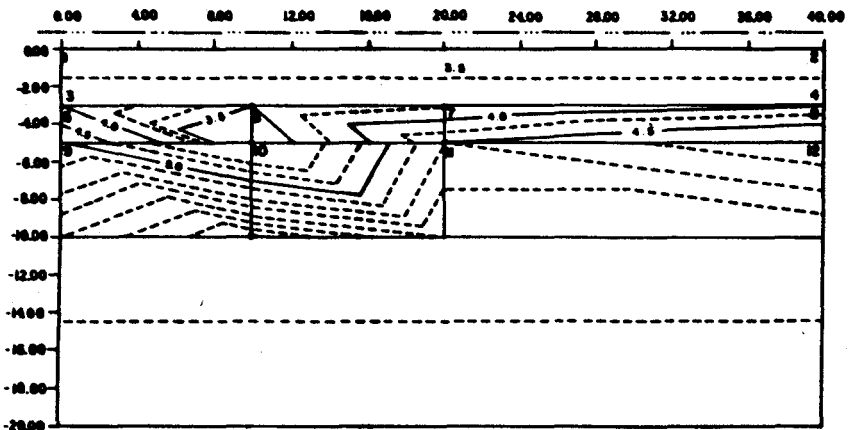
Fig. 9. (a) left: Starting model is $v_1 = v_2 = 3.0$, $v_3 = v_4 = 7.0$; right: resulting model is $v_1 = 3.5$, $v_2 = 4.3$, $v_3 = 6.5$, $v_4 = 7.4$. (b) Convergence of model and residuals are shown in third and second row. The size of models is the same as in the previous example.

iterations were necessary. From this, we conclude that the determination of accurate residuals improved with the inclusion of this term. The convergence history is shown in Figure 9(b).

In model 4 (Figure 10) two discontinuities and a low velocity zone around point number 10 were included. Again, the convergence was perfect in seven iterations, but we could see from the iterative sequence that the process could stop at the fifth. In this example and in model 7, the source was located at the origin.



(a)



(b)

Fig. 10. (a) Starting model for model 4. Discontinuities at $z = -3.0$ and $z = -5.0$ are included. (b) The resulting model (after 7 iterations), which is the same as the actual model.

Several more complicated models were tried, all with similar results. A positive bias was inherent in the problem in the sense that the assumed models had the same discretization as the actual ones. The results of models 1 and 2 show that by including a large enough number of points the demands on the discretization are somewhat relaxed. Still, the number of points to use is not the only important feature. A more critical test was tried in which the discretized models ('actual' and assumed) do not coincide. Conflict is expected in this case, because the iterative solution must be worked out using fixed (rigid) coordinates, and as many as six actual regions could be partially contained in only one assumed region (Figure 11). Using a large number of points for discretization reduces the conflict, but it does not solve it. The incom-

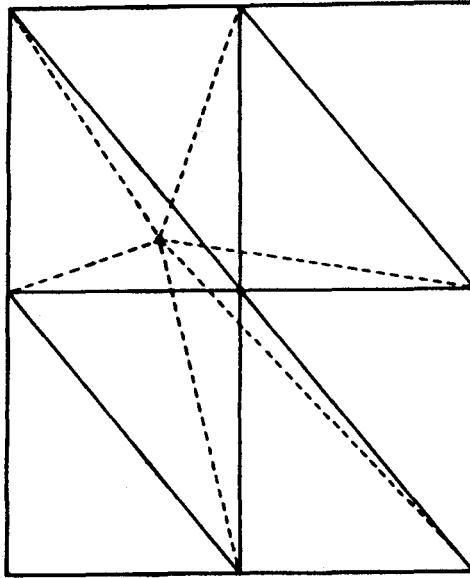


Fig. 11. Example of incompatibilities between the assumed (solid lines) and the actual (broken lines) models.

patibility between assumed and actual model is low, but still it does exist. An improper discretization becomes important if one is concerned with economy. Geological regions which are possibly simple would require few triangles, and in this case, their distribution might be critical. Using always a large number of triangles makes this question irrelevant at the expense of raising computational costs.

A way to deal with this limitation was devised by means of the simple transformation defined by (1). Two different systems of coordinates exist (Figure 12); the space in (a) is referred to as the 'configuration' space, defined by ordered couples

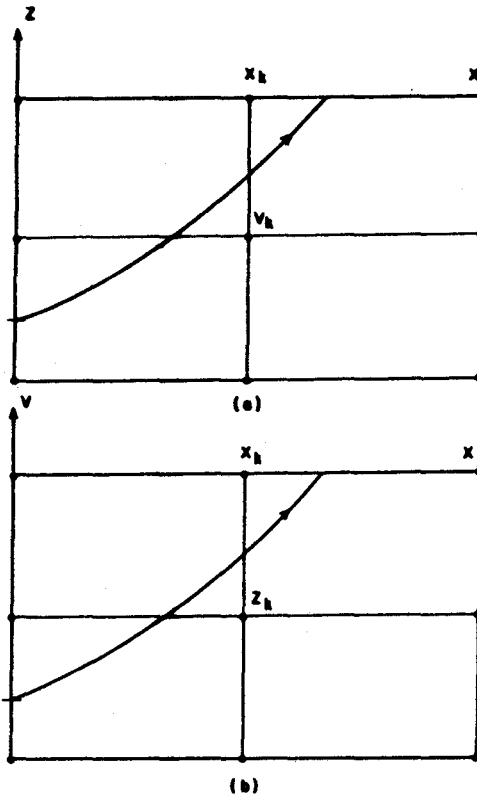


Fig. 12. (a) Isolines of $v(x, z)$. (b) Isolines of $z(x, v)$.

(coordinates) and an associated velocity that satisfy (1). The system shown in (b) will be called 'phase' space, its vertical axis being the velocity. Due to the one-to-one character of (1), every point (x, v) corresponds to a unique value of z . Furthermore, the transformation is symmetric in x, z , and v , thus the description is equivalent in either space. This can be seen by superposing 12(a) and 12(b), since all vectors remain the same as well as the raypath. Thus, inverting in phase space with respect to z is equivalent to inverting in configuration space with respect to v . By (1):

$$\delta T = \left(\frac{\partial T}{\partial v} \right) \delta v = \left(\frac{\partial T}{\partial z} \right) \delta z \tag{29}$$

For each term in the summation (23) we have, from (1)

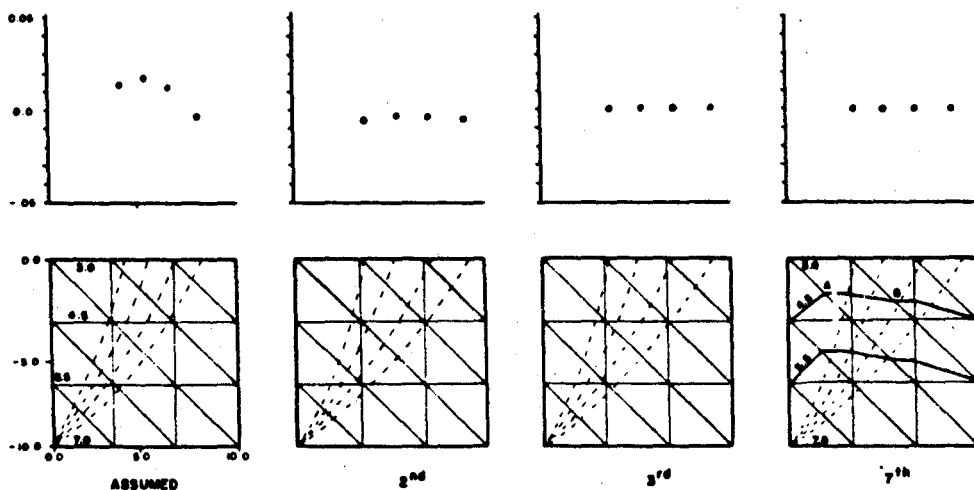
$$\frac{\partial \Delta T_1}{\partial v} = \frac{1}{b_{12}} \frac{\partial \Delta T_1}{\partial z}$$

so that

$$\frac{\partial T}{\partial z} = \sum b_{12} \left(\frac{\partial}{\partial v} (\Delta T_1) \right) \tag{30}$$

From (29) and (30), we conclude that in order to invert in phase space it suffices to exchange v by z , and to weight the regional partial derivatives with their corresponding vertical gradients. The result of this operation in configuration space does not change the velocity at a point, but does perturb the z -coordinate of the isovelocity line with value v along the line $x = \text{const.}$, i. e., it changes the shape of the isovelocity line. Inversion in phase space may also be performed in terms of the x -coordinate as well, so that an alternate (in x and z) scheme may be devised to reduce the incompatibility between the actual and assumed models. Discrepancies originated by the difference in the number of points used to invert will still appear, but better results can be expected. Since one usually cannot draw isovelocities in the earth, these 'better results' are strictly referred to final travel time residuals.

Models 5 and 6, illustrated in figure 13 (a, b), provide a simple example of incompatibility. In model 5 a rigid geometrical grid was used, while in model 6 the inversion was carried out in phase space, keeping the x -isolines constant, so that perfect convergence was expected. The results of inverting model 5 eleven times show that there are regions where the incompatibility could not be resolved. This is due to the fact that the inverted isovelocities must end exactly in the corresponding diagonals of the triangles (points A and B in figure 13 (a)), and the continuity of the isovelocity lines forces their behavior. On the contrary, in model 6, the change of position of the isovelocities includes a change of shape of the triangle regions themselves, so that the technique becomes adaptive. In this example, model 5 converged to the best possible model satisfying the data. Still, comparison of both results is satisfactory.



(a)

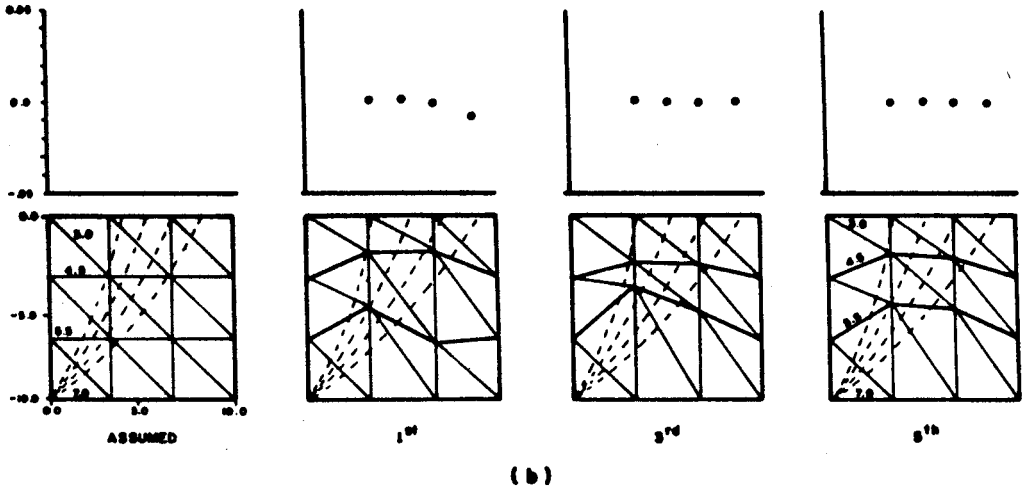
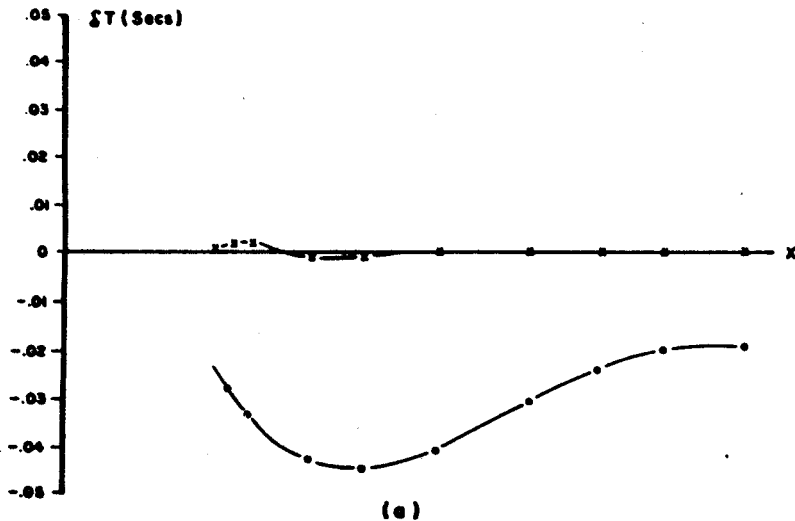


Fig. 13. Model 5. Here the inversion is performed in the (x,z) space, so that the triangles are fixed. Isovelocities for $v = 3.0$ and $v = 4.5$ are shown in the last, resulting model after 7 iterations. (b) Here, the inversion is performed in the 'phase' space. 1: starting model, 2: 1st iteration, 3: 4th iteration, 4: 7th iteration, which coincides with the actual model. Compare with the results in (a).

Several techniques may be developed to attack an inversion problem similar to those in models 5 and 6. An example is given by model 7 (figure 14). Here, solid lines represent the 'actual' model. Broken thin lines are isovelocities of the resulting model, while broken heavy lines are the isovelocities of the initial model. We can see



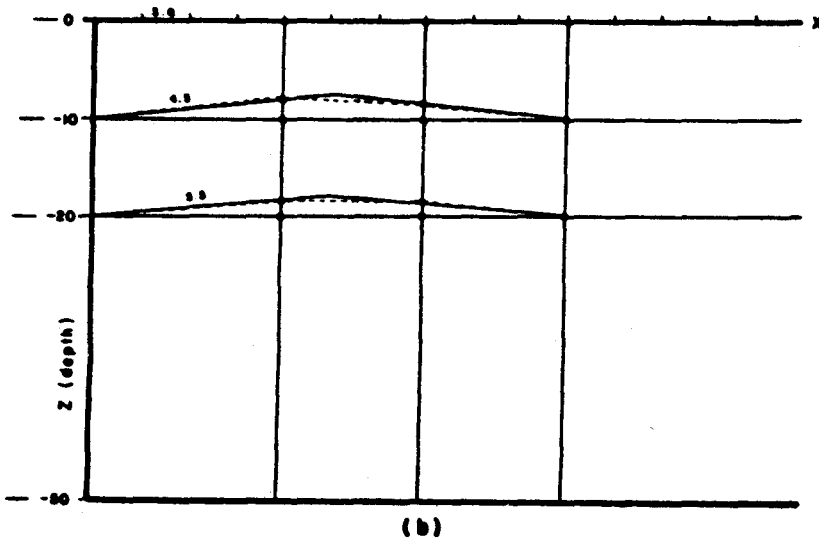


Fig. 14. Example of a simple incompatibility. (a) The dotted curve shows the initial residuals. The crossed curve above it shows the residuals after 7 iterations. (b) The dotted slight line represents the resulting model, while the solid slant line represents the actual model. The horizontal heavy line is the initial, assumed model.

that the inversion raised up the original horizontal isovelocities, although we cannot expect perfect convergence due to the obvious incompatibilities in discretization. A systematic search for the 'actual' position of the central vertical line (defined by the cusps of isovelocities of the 'actual model') would yield better results. Another way to proceed is first to invert for the position of the upper (4.5 in this case) isovelocity line using rays with turning points above it until a stable result is obtained, and then proceed to invert for the next lower isovelocity with any other rays, keeping the first isovelocity fixed. Another possible procedure is to invert both lines simultaneously using only one vertical line positioned between the extremes of the model until a stable result is achieved, and then to add intermediate vertical lines either one by one or several at a time, according to the available data.

BIBLIOGRAPHY

- ARIC, K., GUTDEUTCH and A. SAILER, 1980. Computation of travel times in a medium of two-dimensional velocity distribution. *Pure and Applied Geophysics*, 118, 796-805.
- CERVENY, V., I. A. MOLOTKOV and I. PSCENCICK, 1977. Ray methods in seismology. Charles University, Prague.
- CHAPMAN, C. H., 1978. A new method for computing synthetic seismograms, *Geophys. J. R. Astr. Soc.*, 54, 481-518.

- CHAPMAN, C. H. and R. DRUMMOND, 1982. Body wave seismograms in inhomogeneous media using Maslov Asymptotic Theory, *72*, 6, S277-S317.
- FIRBAS, A., 1981. Inversion of travel time data for laterally heterogeneous velocity structure - linearization approach. *Geophys. J. R. Astr. Soc.* *67*, 189-198.
- GEBRANDE, H., 1976. A seismic tracing method for two-dimensional inhomogeneous media, *in*: Explosion seismology in central Europe: data and results, eds. P. Griese, C. Prodhels and A. Skin, Springer-Verlag, Berlin, pp. 162-167.
- JACKSON, D. D., 1972. Interpretation of inaccurate, insufficient and inconsistent data. *Geophys. J. R. Astr. Soc.*, *28*, 97-109.
- MADRID, J. and C. TRASLOSHEROS, 1983. Un modelo sísmico preliminar lateralmente heterogéneo del campo geotérmico de Cerro Prieto, Baja California Norte, *Geofís. Int.*, *22-4*, 389-417.
- PEREYRA V., W., K. LEE and H. B. KELLER, 1980. Solving two-point seismic ray tracing problems in a heterogeneous medium. Part 1. A general adaptive finite differences method, *Bull. Seism. Soc. Am.*, *70*, 1, 79-99.
- SPENCER, C. and D. GUBBINS, 1980. Travel time inversion for simultaneous earthquake location and velocity structure in laterally varying media. *Geophys. J. R. Astr. Soc.*, *63*, 95-116.
- THURBER, C., 1980. Two-dimensional models of the velocity structure of the crust under the Coyote Lake area, California. Personal communication.
- WIGGINS, R. A., 1976. The general linear inverse problem: implications of surface waves and free oscillations on earth structure, *Rev. Geophys. and Space Phys.*, *10*, 251-258.
- WIGGINS, R. A., 1976. Body wave amplitude calculations II. *Geophys. J. R. Astr. Soc.*, *46*, 1-10.
- WIGGINS, R. A. and J. MADRID, 1974. Body wave amplitude calculations. *Geophys. J. R. Astr. Soc.*, *37*, 423-433.